Correlated line broadening in multidimensional vibrational spectroscopy

Ravindra Venkatramani and Shaul Mukamel[a)]
Departments of Chemistry and Physics and Astronomy, University of Rochester, Rochester, New York 14627

(Received 20 June 2002; accepted 10 September 2002)

The third-order optical response of two coupled anharmonic vibrations interacting with a Brownian oscillator bath that induces energy level fluctuations with arbitrary time scales and degree of correlation is calculated. Two-dimensional correlation plots show distinct signatures of these fluctuations in the various possible three pulse, infrared, femtosecond techniques. © *2002 American Institute of Physics.* [DOI: 10.1063/1.1518001]

I. INTRODUCTION

Coherent, multiple-pulse, nuclear magnetic resonance techniques are widely used to probe the structure and dynamics of complex molecules.[1,2] Similar schemes proposed for the study of vibrational excitations using infrared pulses[3,4] offer a new window into molecular structure with greatly improved (50 fs) temporal resolution.[5–12] Higher order Raman techniques provide a complementary multidimensional view of vibrational dynamics.[3,13–19] By spreading the signal in several dimensions, *n*-wave mixing spectroscopies reveal information about anharmonic couplings, dipole projections, molecular structure, and vibrational relaxation, which is not accessible from conventional linear spectroscopy. A four-wave mixing process involving three input pulses generally provides a three-dimensional projection of the system through the three independent time intervals between pulses (Fig. 1). One can display the information about correlation of events in the various time intervals in the time domain, frequency domain, or using a mixed time frequency representation.

Mapping the spectral features onto the underlying molecular structure[20] has been an important goal of *n*D spectroscopy. Since vibrational motions are greatly influenced by couplings to low frequency, solvent or intramolecular, (bath) degrees of freedom,[6–9,21] a proper analysis of these spectra requires a microscopic treatment of the line broadening induced by this coupling. A multitude of bath time scales usually leads to complicated line shapes and understanding the role of the bath may help in the design of more elaborate, novel pulse sequences. These include using phase control[22,23] or coherent combinations of different techniques that could target a specific goal such as obtaining narrower features, eliminating diagonal peaks, or controlling the ratio of signals of different modes.[24] One interesting future direction is the use of learning algorithms to generate pulses shaped specifically to accomplish a desired goal.[25,26]

In this paper we study effects of correlated line broadening in coupled vibrations and their signatures in two-dimensional (2D) infrared (IR) spectra using a microscopic correlation function theory of four wave mixing line shapes.[27] Using a multilevel system interacting with a harmonic bath we derive closed expressions for the third-order response function and its frequency domain counterpart, the susceptibility $\chi^{(3)}$ in terms of a correlation function matrix $C_{\mu\nu}$ representing energy fluctuations, with arbitrary degree of correlation, of each pair of levels μ and ν. This formalism was applied earlier to compute the electronic nonlinear response of excitons in molecular aggregates where the effects of exciton–phonon interaction on two pulse photon echo signals were studied for different models of bath spectral densities.[28,29] The present work applies this model to the spectroscopy of coupled vibrations.[30] We use a dynamic theory of broadening and adopt the overdamped Brownian oscillator model[31] for the matrix of spectral densities which determine $C_{\mu\nu}(t)$. The spectra are simulated for fast, slow and intermediate bath time scales represented by a parameter κ with an arbitrary degree of correlation between the various collective bath coordinates (anticorrelated, uncorrelated, and fully correlated), represented by a parameter η.

In Sec. II we present the model system of coupled vibrations in both the localized and the exciton basis. In Sec. III we derive correlation function expressions for the third-order response function. The line broadening model is introduced in the localized basis, so that spectral features can be directly related to properties of the physical structure, i.e., specific bonds. Section IV surveys the possible three pulse four wave mixing techniques. In Sec. V we apply the theory to a system of two coupled vibrations and study signatures of the bath in 2D infrared spectra.

II. VIBRATIONAL MODEL HAMILTONIAN

A system of N localized coupled vibrations is described by the Hamiltonian

$$H=\frac{1}{2}\sum_{m=1}^{N}\left(\frac{P_m^2}{M_m}+M_m\omega_m^2X_m^2\right)+\sum_{m=1}^{N}V_mX_m+\sum_{m\neq n=1}^{N}\frac{V_{mn}}{2!}X_mX_n+\sum_{mnk=1}^{N}\frac{V_{mnk}}{3!}X_mX_nX_k+\sum_{mnkl=1}^{N}\frac{V_{mnkl}}{4!}X_mX_nX_kX_l+\cdots, \tag{1}$$

where X_m, P_m, ω_m, and M_m are the coordinate, momentum, frequency, and mass of the mth vibration, respectively, and

a)Electronic mail: mukamel@chem.rochester.edu

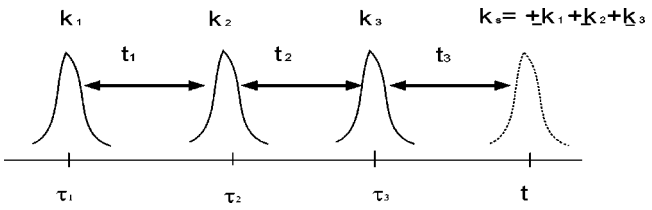

FIG. 1. Pulse sequence for a four wave mixing process. t_1, t_2, and t_3 are the time intervals between the pulses with wave vectors $\mathbf{k_1}$, $\mathbf{k_2}$, $\mathbf{k_3}$, and $\mathbf{k_s}$. The signal is given by one of the eight combinations $\mathbf{k_s}=\pm\mathbf{k_1}\pm\mathbf{k_2}\pm\mathbf{k_3}$ representing distinct multidimensional techniques.

V represent derivatives of the potential energy surface with respect to the local coordinates X_m, which could be chosen to be internal coordinates representing bond stretches, angle bends, and dihedral angle torsions. For assuming a stable geometry we may set $V_m=0$. We quantize the Hamiltonian by introducing creation and annihilation operators B and $B^\dagger$ satisfying the bosonic commutation rules: $[B_m^\dagger,B_n]=\delta_{mn}$ and $[B_m,B_n]=[B_m^\dagger,B_n^\dagger]=0$,

$$X_m=\frac{1}{\sqrt{2M_m\omega_m}}(B_m^\dagger+B_m),$$

$$P_m=-i\sqrt{\frac{M_m\omega_m}{2}}(B_m^\dagger-B_m). \tag{2}$$

The molecular Hamiltonian, truncated to quartic order, can then be written as

$$H=H_0+H'. \tag{3}$$

Here H_0 is a zeroth-order Hamiltonian which preserves the number of excitations,

$$H_0=\sum_{mn=1}^{N} U_n^m B_m^\dagger B_n+\sum_{mnkl=1}^{N} U_{kl}^{mn} B_m^\dagger B_n^\dagger B_k B_l, \tag{4}$$

where

$$U_n^m=\delta_{mn}\left(\omega_n+\frac{1}{2}\sum_{l=1}^{N} U_{ll}^{nn}\right)+\frac{1}{2}(1-\delta_{mn})\left(A_{mn}+\sum_{l=1}^{N} U_{nl}^{ml}\right) \tag{5}$$

and

$$U_{kl}^{mn}=\frac{1}{2!4!4}\sum_{p(mnlk)} A_{mnlk} \tag{6}$$

with

$$A_{mn}=\frac{V_{mn}}{\sqrt{M_m\omega_m M_n\omega_n}}, \tag{7}$$

$$A_{mnlk}=\frac{V_{mnlk}}{\sqrt{M_m\omega_m M_n\omega_n M_l\omega_l M_k\omega_k}} \tag{8}$$

and H' is given by

$$H'=\sum_{mn=1}^{N} U^{mn}B_m^\dagger B_n^\dagger+U_{mn}B_mB_n+\sum_{mnk=1}^{N} U^{mnk}B_m^\dagger B_n^\dagger B_k^\dagger+U_k^{mn}B_m^\dagger B_n^\dagger B_k+U_{nk}^m B_m^\dagger B_nB_k+U_{mnk}B_mB_nB_k+\sum_{mnkl} U_l^{mnk}B_m^\dagger B_n^\dagger B_k^\dagger B_l+U_{nkl}^m B_m^\dagger B_nB_kB_l+\sum_{mnkl} U^{mnkl}B_m^\dagger B_n^\dagger B_k^\dagger B_l^\dagger+U_{mnkl}B_mB_nB_kB_l. \tag{9}$$

In writing H_0 and H', we have used normal ordering of operators, which is convenient for computing matrix elements.[32] The U's are real and satisfy $U_{kl}^{mn}=U_{lk}^{nm}=U_{kl}^{nm}=U_{lk}^{mn}$ and $U_{kl}^{mn}=U_{mn}^{kl}$. Using a basis set of a direct product space of N harmonic oscillators corresponding to the coordinates X_m, we find that H_0 has a block diagonal form with couplings only between states having the same number of quanta. H' provides couplings between states differing by two, three, and four quanta. For peptides and metal carbonyl complexes like RDC[33,34] the coupling between the states differing by two quanta is about two orders of magnitude smaller than the frequency difference between the states and has a small effect on shifting the energies of the states. Hereafter we therefore only consider the dominant resonant contributions to the third-order signal. We only keep the quartic anharmonicities and neglect H', retaining only the zeroth-order Hamiltonian H_0. Inclusion of cubic anharmonicities may lead to additional interesting features[13,35] but we do not consider these here.

Our vibrational system is further coupled to a harmonic (phonon) bath described by the Hamiltonian

$$H_{\mathrm{ph}}=\frac{1}{2}\sum_j \frac{p_j^2}{m_j}+m_j\omega_j^2 q_j^2 \tag{10}$$

and the system bath coupling H_c is assumed to be linear in bath coordinates and quadratic and quartic in system coordinates. We assume the solvent and system vibrational frequencies are well separated so that bilinear couplings (q_jX_m) giving rise to population relaxation are negligible.[36] We therefore adopt the following form for the coupling:

$$H_c\sim\sum_{mn=1}^{N} q_{mn}^{(c)}X_mX_n+\sum_{mnkl=1}^{N} q_{mnkl}^{(c)}X_mX_nX_kX_l. \tag{11}$$

Here $q^{(c)}$ are collective bath coordinates

$$q_{mn}^{(c)}=\sum_j m_j\omega_j z_{j,mn}q_j, \quad q_{mnkl}^{(c)}=\sum_j m_j\omega_j z_{j,mnkl}q_j \tag{12}$$

with $z_{j,mn}$ and $z_{j,mnkl}$ representing the coupling strength between the jth bath mode and the vibrations. Recasting the coupling using the creation/annihilation operators leads to resonant terms of the type $qB^\dagger B$ which induce frequency fluctuations and off-resonant terms of the type $qB^\dagger B^\dagger$ or qBB leading to population relaxation. In the weak coupling regime the off-resonant terms can be neglected[37] and we have

$$H_c = \sum_{mn=1}^{N} q_{mn}^{(c)} B_m^\dagger B_n + \sum_{mnkl=1}^{N} q_{mnkl}^{(c)} B_m^\dagger B_n^\dagger B_k B_l . \tag{13}$$

The total Hamiltonian for the optically driven vibrations coupled to the bath is finally given by

$$H = H_0 + H_{\rm ph} + H_c - \mathbf{E}(t)\cdot\mathbf{P}, \tag{14}$$

where the last term represents the coupling to the radiation field $E(t)$. The dipole moment operator is assumed to be linear in the vibrational coordinates

$$\mathbf{P} = \sum_{m=1}^{N} \mathbf{d}_m (B_m^\dagger + B_m), \tag{15}$$

where $\mathbf{d}_m$ is the transition dipole of the mth mode.

Calculation of the nonlinear response will be carried out by a transformation to the exciton basis set which diagonalizes the molecular Hamiltonian. Since H_0 is block diagonal, we can diagonalize the single and double excitation blocks separately. Diagonalizing the single excitation block results in the following single exciton states denoted $\alpha, \beta, \gamma, \delta$:

$$|\alpha\rangle \equiv B_\alpha^\dagger |0\rangle = \sum_{m=1}^{N} \phi_{\alpha,m} B_m^\dagger |0\rangle, \tag{16}$$

where $B_\alpha^\dagger$ is the single exciton creation operator. The single exciton wave functions $\phi_{\alpha,m}$ satisfy the normalization relation

$$\sum_{m=1}^{N} \phi_{\alpha,m}\phi_{\beta,m} = \delta_{\alpha\beta} . \tag{17}$$

The double exciton states will be denoted μ, ν:

$$|\mu\rangle \equiv Y_\mu^\dagger |0\rangle = \sum_{\substack{mn=1 \\ n\geqslant m}}^{N} \psi_{\mu,mn} B_m^\dagger B_n^\dagger |0\rangle. \tag{18}$$

Here $Y_\mu^\dagger$ represents the double exciton creation operator and the expansion coefficients $\psi_{\mu,mn}$ are normalized as

$$\sum_{\substack{mn=1 \\ n\geqslant m}}^{N} \psi_{\mu,mn}\psi_{\nu,mn} = \delta_{\mu\nu} . \tag{19}$$

We shall not consider triple and higher exciton bands in our calculations. The total Hamiltonian in the exciton basis is finally given by

$$H_e = H_{0e} + H_{\rm ph} + H_{ce} - \mathbf{E}(t)\cdot\mathbf{P}_e , \tag{20}$$

where

$$H_{0e} = \sum_\alpha E_\alpha B_\alpha^\dagger B_\alpha + \sum_\mu E_\mu Y_\mu^\dagger Y_\mu . \tag{21}$$

H_{ce} is nondiagonal in this basis and this results in a small coupling $q_{\alpha\beta}^{(c)}$ between the excitonic states, as outlined in Appendix A. We neglect this coupling and set[29]

$$H_{ce} = \sum_\alpha q_{\alpha\alpha}^{(c)} B_\alpha^\dagger B_\alpha + \sum_\mu q_{\mu\mu}^{(c)} Y_\mu^\dagger Y_\mu . \tag{22}$$

The dipole moment operator is

$$\mathbf{P}_e = \sum_{\alpha=1}^{N} \mathbf{d}_\alpha (B_\alpha^\dagger + B_\alpha). \tag{23}$$

Here $\mathbf{d}_\alpha$ is the transition dipole from the ground state to the single exciton state α. All our calculations are based on Eqs. (20)–(23) together with Eq. (10).

III. THE THIRD-ORDER RESPONSE

In a four wave mixing experiment the electric field is given by the superposition of three input pulses (Fig. 1),

$$E(\mathbf{r},t) = \sum_{j=1}^{3} [\mathbf{E}_j(t)\exp(i\mathbf{k}_j\mathbf{r} - i\omega_j t) + \mathbf{E}_j^*(t)\exp(-i\mathbf{k}_j\mathbf{r} + i\omega_j t)], \tag{24}$$

where $\mathbf{E}_j$, k_j, and ω_j represent the complex envelope, wave vector, and frequency of the jth pulse. The optical response function $R(t_3,t_2,t_1)$ relates the third-order nonlinear polarization $P^3(t)$ to the driving field $E(t)$:[31]

$$P^3(t) = \int_0^\infty dt_3 \int_0^\infty dt_2 \int_0^\infty dt_1 R(t_3,t_2,t_1) \times E_1(t-t_3)E_2(t-t_3-t_2)E_3(t-t_3-t_2-t_1). \tag{25}$$

The response function is given by a sum of eight terms:[31]

$$R(t_3,t_2,t_1) = \left(\frac{i}{\hbar}\right)^3 \sum_{i=1}^{4} [R_i(t_3,t_2,t_1) - R_i^*(t_3,t_2,t_1)], \tag{26}$$

where each R_i represents a distinct *Liouville space pathway* with its own characteristic resonances

$$\begin{aligned} R_1(t_3,t_2,t_1) &= F(t_1, t_1+t_2, t_1+t_2+t_3, 0), \\ R_2(t_3,t_2,t_1) &= F(0, t_1+t_2, t_1+t_2+t_3, t_1), \\ R_3(t_3,t_2,t_1) &= F(0, t_1, t_1+t_2+t_3, t_1+t_2), \\ R_4(t_3,t_2,t_1) &= F(t_1+t_2+t_3, t_1+t_2, t_1, 0). \end{aligned} \tag{27}$$

t_1, t_2, t_3 are the successive time intervals between pulses (Fig. 1) and F is the four point correlation function:

$$F(\tau_4,\tau_3,\tau_2,\tau_1) = \langle P(\tau_4)P(\tau_3)P(\tau_2)P(\tau_1)\rangle. \tag{28}$$

Substituting the dipole operator [Eq. (23)] into Eq. (28) and noting that F vanishes for combinations involving different number of creation and annihilation operators we get[28]

$$F(\tau_4,\tau_3,\tau_2,\tau_1) = F_1(\tau_4,\tau_3,\tau_2,\tau_1) + F_2(\tau_4,\tau_3,\tau_2,\tau_1), \tag{29}$$

$$F_1(\tau_4,\tau_3,\tau_2,\tau_1) = \sum_{\alpha\beta\gamma\delta} d_\alpha d_\beta d_\gamma d_\delta \langle B_\alpha(\tau_4) B_\beta^\dagger(\tau_3) \times B_\gamma(\tau_2) B_\delta^\dagger(\tau_1)\rangle, \tag{30}$$

$$F_2(\tau_4,\tau_3,\tau_2,\tau_1) = \sum_{\alpha\beta\gamma\delta} d_\alpha d_\beta d_\gamma d_\delta \langle B_\alpha(\tau_4) B_\beta(\tau_3) \times B_\gamma^\dagger(\tau_2) B_\delta^\dagger(\tau_1)\rangle. \tag{31}$$

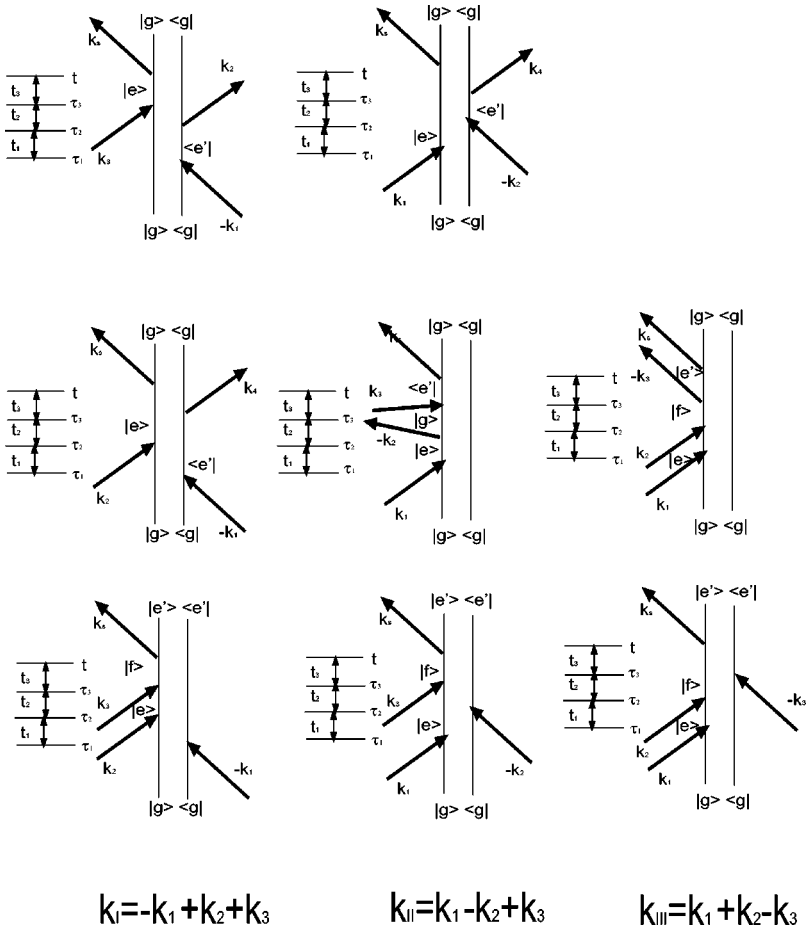

FIG. 2. Double-sided Feynman diagrams representing *Liouville space pathways* contributing to the third-order response for the energy level scheme in Fig. 2. Each column shows diagrams for a particular choice of $\mathbf{k}_s$ as indicated. Only three wave vectors are allowed within the RWA.

Here F_1 represents the contribution of Liouville space pathways which only include single exciton states whereas F_2 represents the contribution of double exciton states. To compute the four point correlation function we first expand F_1 and F_2 in the exciton basis. The expression for F_2 contains terms such as $B_\alpha^\dagger B_\beta^\dagger|0\rangle \equiv |\alpha\beta\rangle$. In general these direct products of single exciton states (obtained by acting the creation operator twice) are not eigenstates of the system. However, the double exciton eigenstates can be expanded in this direct product basis

$$|\mu\rangle = \sum_{\substack{\alpha\beta \\ \beta \geqslant \alpha}} \chi'_{\mu,\alpha\beta}|\alpha\beta\rangle \tag{32}$$

and the inverse transformation is defined as

$$|\alpha,\beta\rangle = \sum_{\mu} \chi_{\mu,\alpha\beta}|\mu\rangle. \tag{33}$$

Normalization implies

$$\chi_{\mu,\alpha\beta} = \sum_{\substack{mn \\ n \geqslant m}} \phi_{\alpha,m}\phi_{\beta,n}\psi_{\mu,mn}, \tag{34}$$

$$\chi'_{\mu,\alpha\beta} = (\chi_{\mu,\alpha\beta})^{-1}. \tag{35}$$

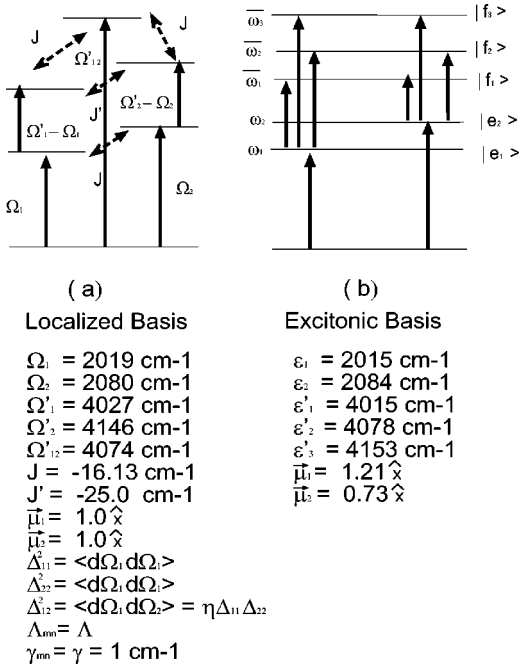

FIG. 3. Energy level scheme for two coupled anharmonic vibrations: (a) The localized basis, (b) the exciton basis, where *e* represents the single exciton manifold and *f* represents the double exciton manifold.

TABLE I. All allowed transitions and relative peak strengths.

Peaks (cm^{-1}, cm^{-1})	Relative peak kinetics $\mathbf{k_I}$	$\mathbf{k_{II}}$	$\mathbf{k_{III}}$	Peaks (cm^{-1}, cm^{-1})	Relative peak intensities $\mathbf{k_I}$	$\mathbf{k_{II}}$	$\mathbf{k_{III}}$
$(\varepsilon_1,\varepsilon_2)$(2015, 2015)	0.971	1.000	1.000	$(\varepsilon_2,\varepsilon_1)$(2084, 2015)	0.349	0.157	0.157
$(\varepsilon_1,\varepsilon_2)$(2015, 2084)	0.343	0.156	0.156	$(\varepsilon_2,\varepsilon_2)$(2084, 2084)	0.129	0.261	0.261
$(\varepsilon_1,\varepsilon_1'-\varepsilon_1)$(2015, 2000)	1.000	0.764	0.764	$(\varepsilon_2,\varepsilon_1'-\varepsilon_1)$(2084, 2000)	0.733	0.101	0.101
$(\varepsilon_1,\varepsilon_1'-\varepsilon_2)$(2015, 1931)	0.006	0.077	0.078	$(\varepsilon_2,\varepsilon_1'-\varepsilon_2)$(2084, 1931)	0.099	0.011	0.011
$(\varepsilon_1,\varepsilon_2'-\varepsilon_1)$(2015, 2063)	0.349	0.147	0.147	$(\varepsilon_2,\varepsilon_2'-\varepsilon_1)$(2084, 2063)	0.021	0.169	0.169
$(\varepsilon_1,\varepsilon_2'-\varepsilon_2)$(2015, 1994)	0.121	0.154	0.154	$(\varepsilon_2,\varepsilon_2'-\varepsilon_2)$(2084, 1994)	0.308	0.136	0.136
$(\varepsilon_1,\varepsilon_3'-\varepsilon_1)$(2015, 2138)	0.071	0.015	0.015	$(\varepsilon_2,\varepsilon_3'-\varepsilon_1)$(2084, 2138)	0.003	0.074	0.074
$(\varepsilon_1,\varepsilon_3'-\varepsilon_2)$(2015, 2069)	0.087	0.037	0.037	$(\varepsilon_2,\varepsilon_2'-\varepsilon_1)$(2084, 2069)	0.105	0.142	0.142

Using these expressions and the second-order cumulant expansion, we can evaluate Eqs. (30) and (31)[28] and recast them in terms of the two point correlation functions of the collective coordinates

$$C_{ab}(t)=\frac{1}{\hbar^2}\langle q_a^{(c)}(t)q_b^{(c)}(0)\rangle, \quad a,b=mn,mnkl. \tag{36}$$

In the Brownian oscillator model, each collective coordinate satisfies the Langevin equation:

$$\ddot{q}_a^{(c)}+\gamma_a\dot{q}_a^{(c)}+\omega_a q_a^{(c)}=f_a(t)+F_a(t), \tag{37}$$

where γ_a and ω_a represent the friction and the characteristic frequency associated with the ath collective mode. The oscillator is driven by the force associated with the external field F_a and a Gaussian random force f_a. Typically solvent motions are overdamped and the characteristic frequencies are low compared to the friction coefficient ($\gamma_a \gg \omega_a$). In the high temperature limit ($\omega_a \ll K_BT$) the correlation function assumes the form:[31]

$$C_{ab}(t)=\left[\frac{2K_BT\lambda_{ab}}{\hbar}-i\lambda_{ab}\Lambda_{ab}\right]\exp(-\Lambda_{ab}t) \tag{38}$$

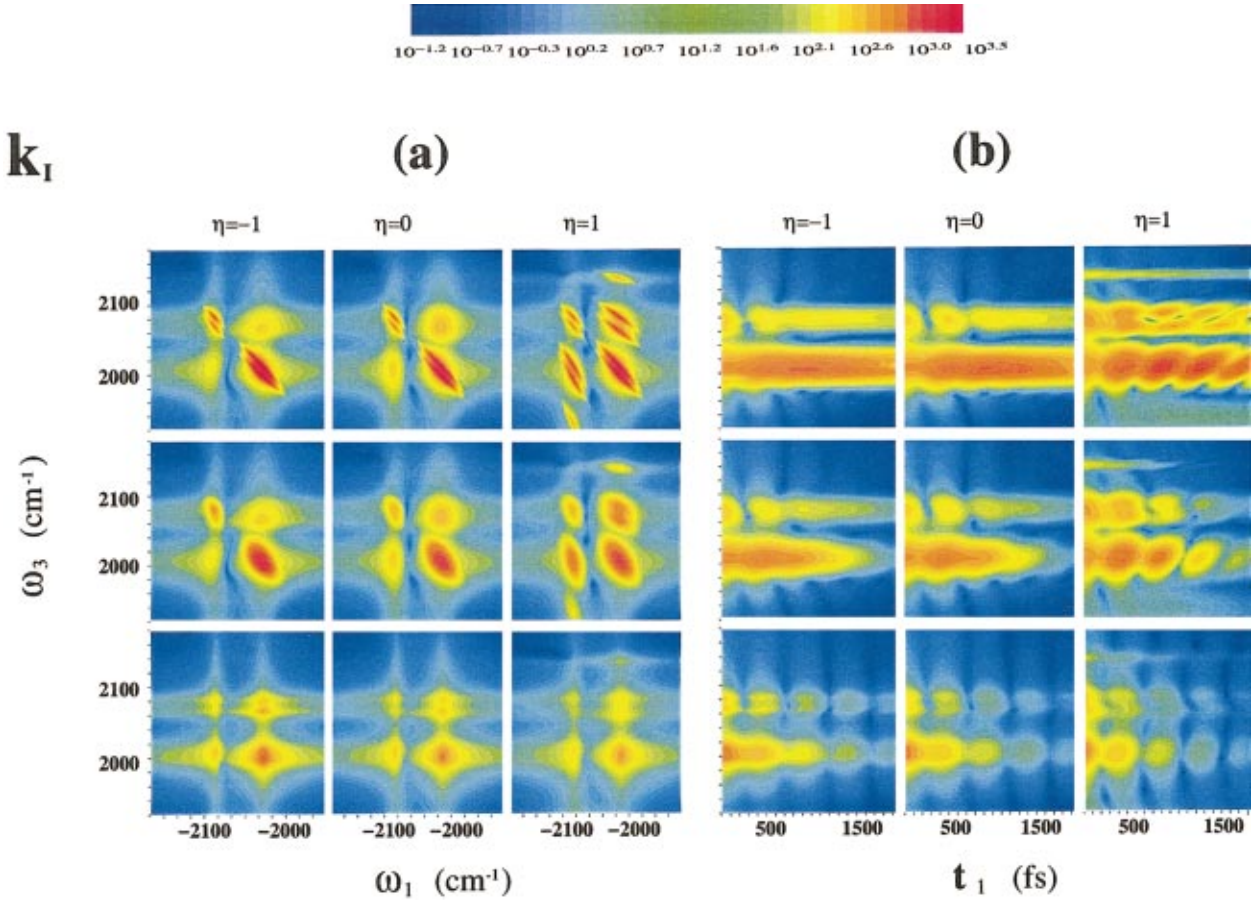

FIG. 4. (Color) (a) The homodyne frequency domain 2D signal $S(\omega_3,t_2=0,\omega_1)$ and (b) the homodyne mixed time-frequency domain 2D signal $S(\omega_3,t_2=0,t_1)$ for $\mathbf{k_I}$, both on a logarithmic scale. First, second, and third rows represent the slow bath limit ($\kappa_1=8.4\times10^{-5}$; $\kappa_2=1.3\times10^{-4}$), the intermediate bath limit ($\kappa_1=0.083$; $\kappa_2=0.1312$), and the fast bath limit ($\kappa_1=3.114$; $\kappa_2=3.99$), respectively.

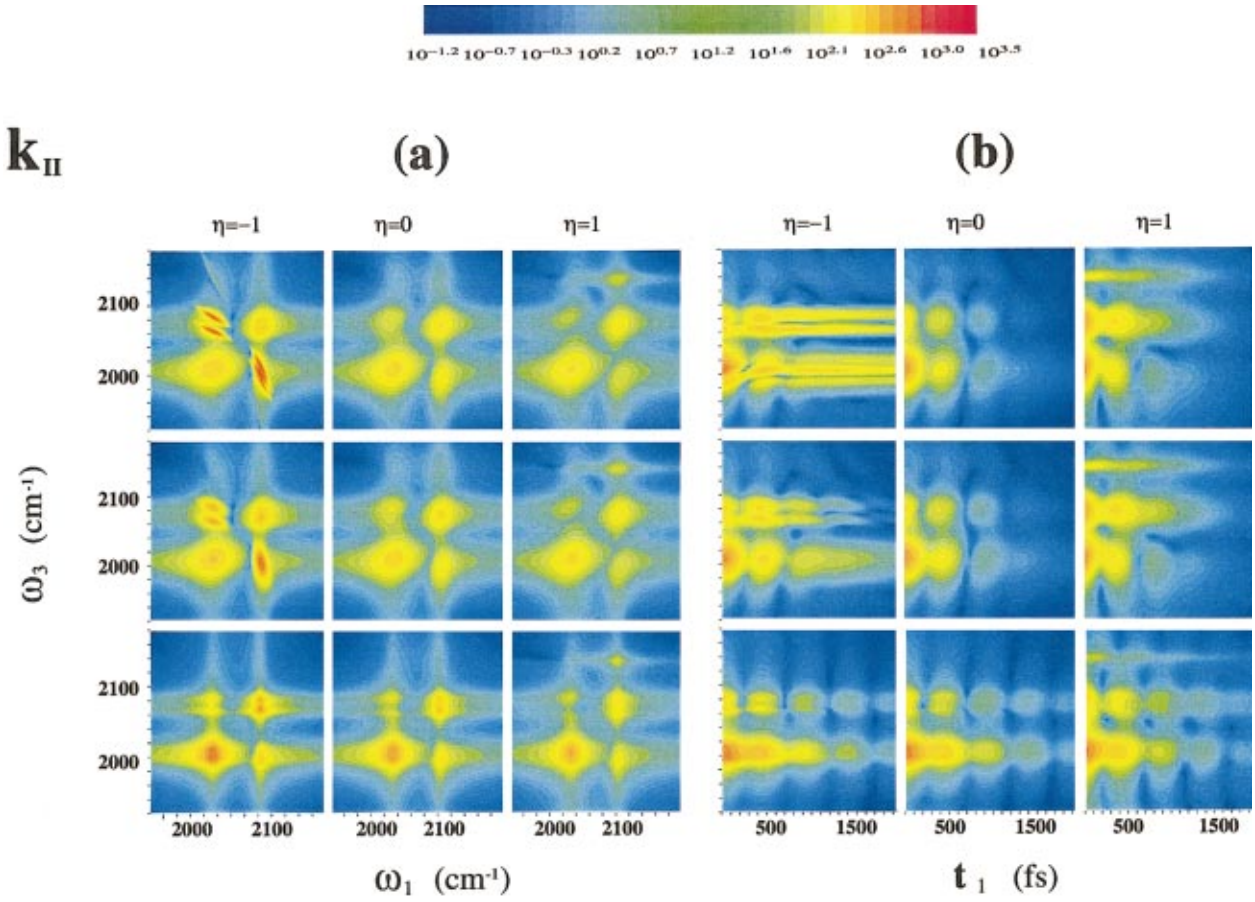

FIG. 5. (Color) Same as Fig. 4 but for $\mathbf{k_{II}}$.

with $a,b=mn,mnkl$. Here λ_{ab} is the reorganization energy associated with the ab collective coordinate and Λ_{ab} represents the inverse time scale of its fluctuations. We further define the parameter $\Delta_{ab}^2 \equiv \langle q_a^{(c)} q_b^{(c)} \rangle = 2K_B T \lambda_{ab}/\hbar$. Δ_{aa} represents the magnitude of fluctuations of the energy of states a, while the off-diagonal elements Δ_{ab} represent correlations between the fluctuation amplitudes of different elements of the molecular Hamiltonian. In electronic spectroscopy the imaginary part of Eq. (38) is responsible for the fluorescence Stokes shift. For vibrations however, Λ_{ab} are typically small compared to $K_B T/\hbar$ and the imaginary part may often be neglected.

From the Cauchy–Schwartz inequality we have $\Delta_{ab}^2 \leqslant \Delta_{aa}\Delta_{bb}$, and we can therefore write

$$\Delta_{ab}^2 = \eta_{ab}\Delta_{aa}\Delta_{bb}. \tag{39}$$

The parameter $-1 \leqslant \eta_{ab} \leqslant 1$ which controls the correlation of fluctuation amplitudes of various levels takes values between -1 (anticorrelated) through 0 (uncorrelated) to 1 (fully correlated).

The final expressions for F_1 and F_2, given in Appendix B, simplify considerably in the two extreme cases of fast and slow baths. We define a parameter $\kappa_{ab} \equiv \Lambda_{ab}/\Delta_{ab}$ which is the ratio of the inverse time scale of the bath to the amplitude of fluctuations. In the slow bath limit ($\kappa \ll 1$) the broadening is characterized by a Gaussian line shape. In the fast bath limit ($\kappa \gg 1$) the correlations between the different collective coordinates decay very rapidly resulting in Lorentzian line shapes. Closed expressions for F_1 and F_2 in both limits are given in Appendix C.

IV. SURVEY OF THE 2D SIGNALS

The pulse configuration in a four wave mixing experiment [Eq. (24)] is shown in Fig. 1. The signal can be detected in any of the eight directions given by a linear combination of the input pulses $\mathbf{k_s} = \pm\mathbf{k_1} \pm \mathbf{k_2} \pm \mathbf{k_3}$. Four distinct techniques are possible ($\mathbf{k_I} = -\mathbf{k_1} + \mathbf{k_2} + \mathbf{k_3}$, $\mathbf{k_{II}} = \mathbf{k_1} - \mathbf{k_2} + \mathbf{k_3}$, $\mathbf{k_{III}} = \mathbf{k_1} + \mathbf{k_2} - \mathbf{k_3}$, and $\mathbf{k_{IV}} = \mathbf{k_1} + \mathbf{k_2} + \mathbf{k_3}$). Calculations of the third-order response are simplified once $\mathbf{k_s}$ is specified. Since the choice of a particular $\mathbf{k_s}$ also implies a particular combination of field frequencies $\omega_s = \pm\omega_1 \pm \omega_2 \pm \omega_3$ only some of the contributions to the third-order response will be fully resonant with all fields, the others are highly oscillatory and will be neglected by invoking the rotating wave approximation (RWA). Only the first three techniques survive the RWA for our model and the corresponding double sided Feynman diagrams are shown in Fig. 2.[31] $\mathbf{k_I}$ and $\mathbf{k_{II}}$ have two single exciton and one double exciton contribution while $\mathbf{k_{III}}$ has two double exciton contributions. The response function for $\mathbf{k_I}$ is $(i/\hbar)R^I$, where

$$R^I = R_2 + R_3 - R_1^*, \tag{40}$$

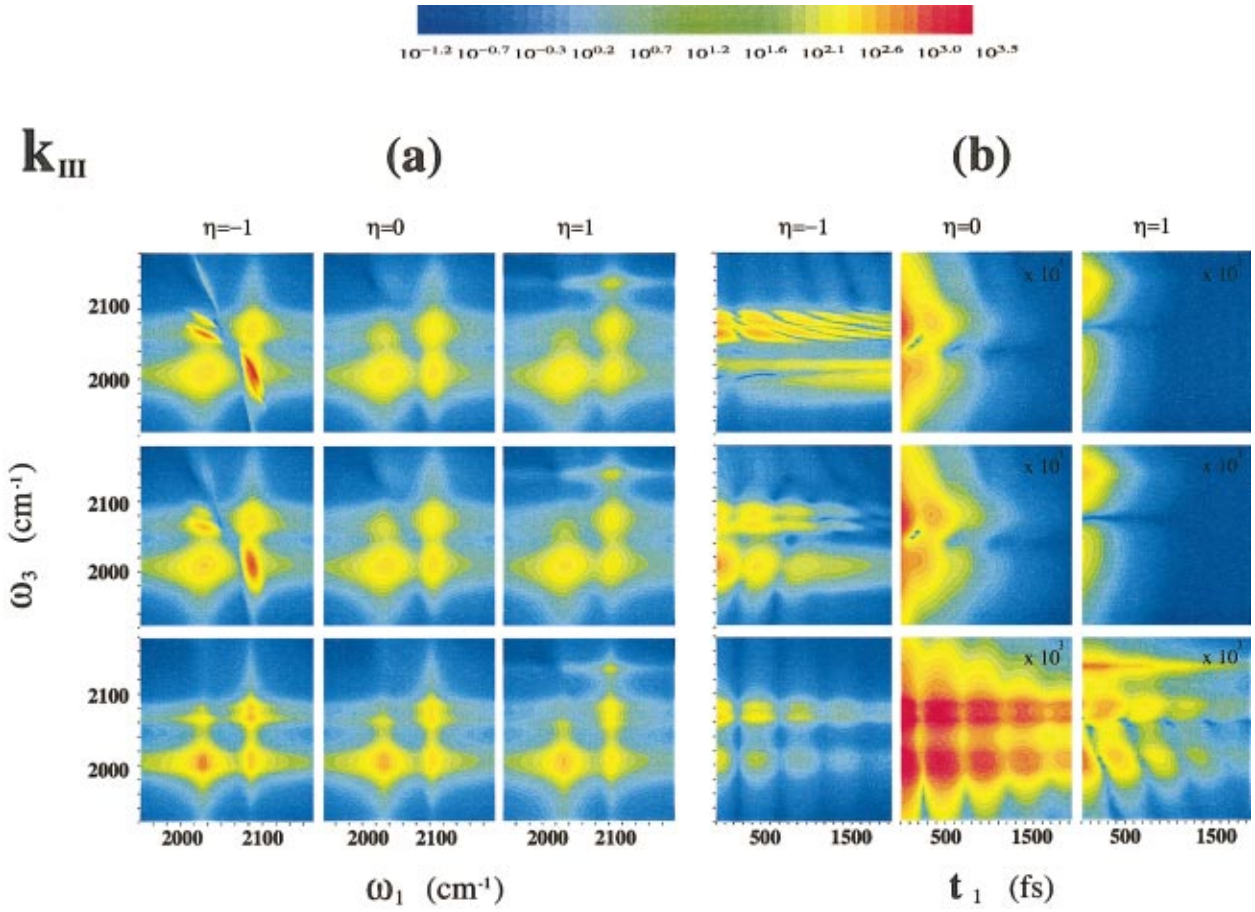

FIG. 6. (Color) Same as Fig. 4 but for $\mathbf{k_{III}}$.

$$R^{\mathrm{I}}(t_3,t_2,t_1)=F_1(0,t_1+t_2,t_1+t_2+t_3,t_1)+F_1(0,t_1,t_1+t_2+t_3,t_1+t_2)-F_2(0,t_1+t_2+t_3,t_1+t_2,t_1).$$

Similarly, for $\mathbf{k_{II}}$ we get

$$R^{\mathrm{II}}=R_1+R_4-R_2^*,\quad R^{\mathrm{II}}(t_3,t_2,t_1)=F_1(t_1,t_1+t_2,t_1+t_2+t_3,0)+F_1(t_1+t_2+t_3,t_1+t_2,t_1,0)-F_2(t_1,t_1+t_2+t_3,t_1+t_2,0). \tag{41}$$

Finally for $\mathbf{k_{III}}$ we have

$$R^{\mathrm{III}}=R_4-R_3^*,\quad R^{\mathrm{III}}(t_3,t_2,t_1)=F_2(t_1+t_2+t_3,t_1+t_2,t_1,0)-F_2(t_1+t_2,t_1+t_2+t_3,t_1,0). \tag{42}$$

We limit our simulations to impulsive techniques where the pulses are shorter than all bath time scales. The signal S_s associated with each choice of wave vector $\mathbf{k_s}$ depends on the response function and the detection mode. We have calculated the following homodyne signal:

$$S_s(\omega_3,t_2,\omega_1)=|(R^s(\omega_3,t_2,\omega_1)|^2, \tag{43}$$

where

$$R^s(\omega_3,t_2,\omega_1)=\int_0^\infty dt_3\int_0^\infty dt_1 R^s(t_3,t_2,t_1)\times\exp(-i(\omega_3t_3+\omega_1t_1)). \tag{44}$$

The 2D (ω_1,ω_3) plots of Eq. (44) for various values of t_2 provide a frequency domain representation. We further computed

$$S_s(\omega_3,t_2,t_1)=|R^s(\omega_3,t_2,t_1)|^2, \tag{45}$$

where

$$R^s(\omega_3,t_2,t_1)=\int_0^\infty dt_3 R^s(t_3,t_2,t_1)\exp(i\omega_3t_3). \tag{46}$$

The 2D (ω_3,t_1) plots then give a mixed time-frequency representation.

We have further examined the real and the imaginary components of the response function which are available from heterodyne detection

$$S_s^R(\omega_3,t_2,\omega_1)=\mathrm{Re}[R^s(\omega_3,t_2,\omega_1)] \tag{47}$$

and

$$S_s^{\mathrm{I}}(\omega_3,t_2,\omega_1)=\mathrm{Im}[R^s(\omega_3,t_2,\omega_1)]. \tag{48}$$

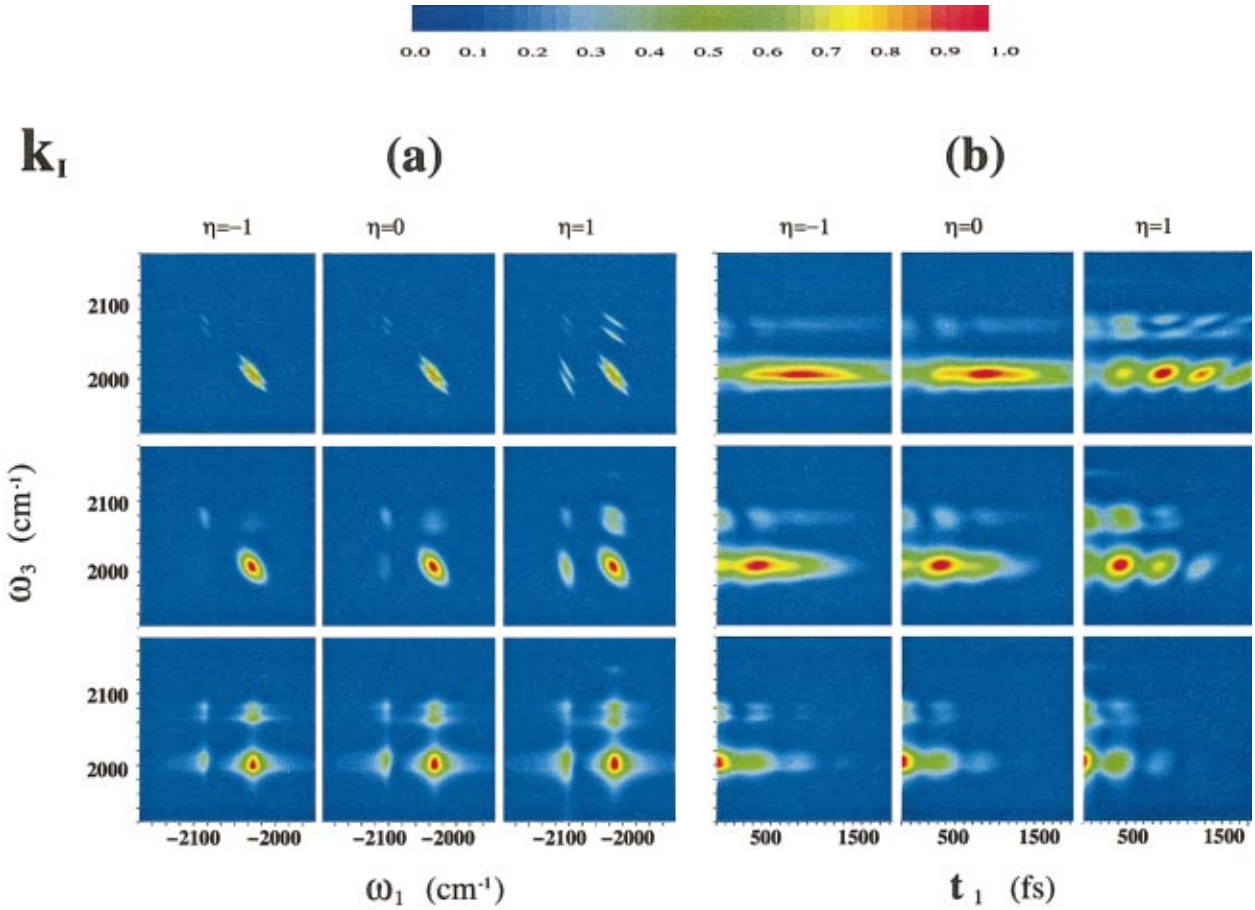

FIG. 7. (Color) The (a) frequency and (b) mixed time-frequency domain signals from Fig. 4 plotted on a linear scale for $\mathbf{k_I}$.

V. APPLICATION TO TWO COUPLED VIBRATIONS

Numerical simulations were performed for a system of two coupled vibrations labeled 1 and 2. This model could represent, for example, the two carbonyl stretches in the amide-I bands in dipeptides[38,39] or in the metal carbonyl complex $Rh(CO)_2(C_5H_7O_2)$ (RDC).[33,34] The zero-order energy level scheme for our model in the localized basis set is shown in Fig. 3(a). The first excited states have energies $\Omega_1 \equiv U_1^1 = 2019\ \mathrm{cm}^{-1}$ and $\Omega_2 \equiv U_2^2 = 2080\ \mathrm{cm}^{-1}$ with overtones $\Omega_1' \equiv U_{11}^{11} = 4027\ \mathrm{cm}^{-1}$, $\Omega_2' \equiv U_{22}^{22} = 4146\ \mathrm{cm}^{-1}$ and the combination band $\Omega_{12}' = \Omega_1 + \Omega_2 + 4U_{12}^{12} = 4074\ \mathrm{cm}^{-1}$. The couplings between the fundamental levels are $J \equiv U_1^2 = -16\ \mathrm{cm}^{-1}$ and those between the overtones as $J' \equiv U_{11}^{22} = -25\ \mathrm{cm}^{-1}$. The transition dipoles d_m [Eq. (18)] for the two oscillators are parallel and all levels have the same lifetime broadening $\gamma = 1\ \mathrm{cm}^{-1}$. The excitonic basis obtained by diagonalizing this Hamiltonian [Fig. 3(b)] shows two single exciton states at $\epsilon_1 = 2015$ and $\epsilon_2 = 2084\ \mathrm{cm}^{-1}$ and three double exciton states at $\epsilon_1' = 4015$, $\epsilon_2' = 4078$, and $\epsilon_3' = 4153\ \mathrm{cm}^{-1}$. For these parameters the exciton energies resemble those of the carbonyl stretches in RDC.[33]

We assumed that the only relevant collective bath coordinates are q_{11} and q_{22}, which implies that the couplings between the different levels (off-diagonal terms in the Hamiltonian H_0) and anharmonicities do not fluctuate, and used the same relaxation rate ($\Lambda = \Lambda_{11} = \Lambda_{22}$) for these coordinates. This leaves four independent parameters Δ_{11}^2 and Δ_{22}^2, their correlation parameter η: $\Delta_{12}^2 = \eta \Delta_{11} \Delta_{22}$, and Λ. All other fluctuation amplitudes and their correlations can be obtained from these quantities and are listed in Appendix D.

Δ_{mm} and κ_m determine the linewidth (full width at half maximum), Γ_m, for the linear absorption peak at Ω_m (m=1,2),[29]

$$\frac{\Gamma_m}{\Delta_{mm}} = \frac{2.355 + 1.76\kappa_m}{1 + 0.85\kappa_m + 0.88\kappa_m^2}, \tag{49}$$

where $\kappa_m = \Lambda_{mm}/\Delta_{mm}$. In the following calculations we have varied Δ and Λ so as to keep the linewidths of the two independent frequencies fixed $\Gamma_1 = 28\ \mathrm{cm}^{-1}$ and $\Gamma_2 = 18\ \mathrm{cm}^{-1}$.[40]

All calculated 2D signals assume that the second and third pulse were coincident, setting $t_2 = 0$. We expect two possible resonances (ϵ_1; ϵ_2) during t_1 and eight during t_3.[41] The peaks for different techniques along with their intensities are listed in Table I. Figure 4(a) shows contour plots of the $S_s(\omega_3, t_2 = 0, \omega_1)$ signal [Eq. (43)] for $\mathbf{k_I}$ on a log scale. Each column represents different values of the correlation parameter η, whereas the various rows correspond to a different value of the time scale parameter κ. For these parameters the imaginary part of Eq. (38) is completely negligible for the slow and intermediate limits of κ, but makes some contribution in the fast bath limit. These calculations were repeated for techniques $\mathbf{k_{II}}$ (Fig. 5) and $\mathbf{k_{III}}$ (Fig. 6).

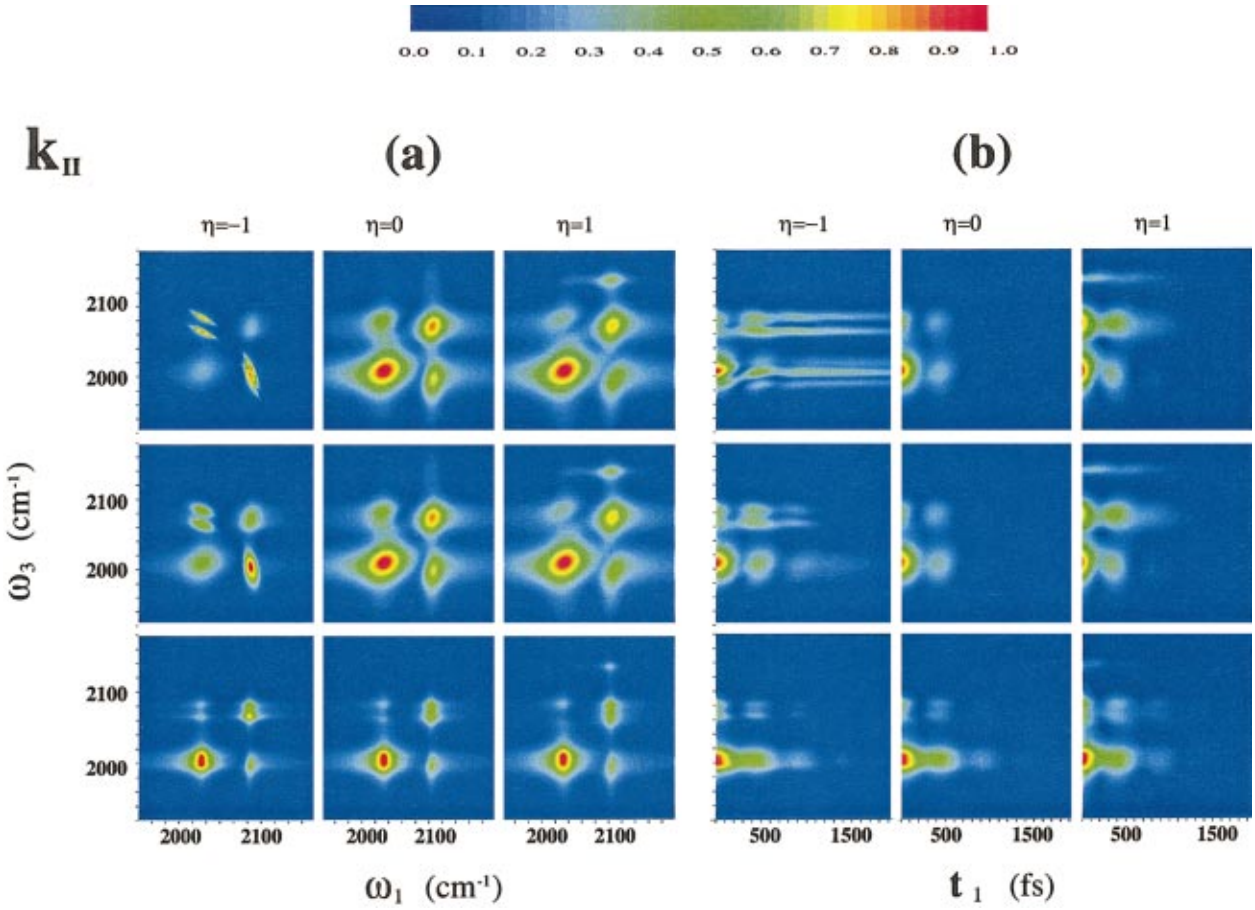

FIG. 8. (Color) Same as Fig. 7 but for $\mathbf{k_{II}}$.

The orientation of the contours provide distinct signatures of the correlation between energy level fluctuations in the slow bath limit for each technique (first row: Figs. 4–6). Anticorrelated (correlated) cross peak contours are oriented along the off-diagonal (diagonal) directions of the axes. Since the anharmonicities are not coupled to the bath and do not fluctuate, the diagonal peak contours are always oriented along the diagonal of the axes in all cases.

Anticorrelated energy level fluctuations reverse the dephasing and rephasing of oscillators in the third time interval t_3 and show distinct signatures in the 2D plots: Anticorrelated cross peaks are poorly resolved compared with correlated peaks for $\mathbf{k_I}$ where an echo signal is expected in the third time interval due to the rephasing of oscillators. The intense (2015; 2138) peak for $\eta=1$ is absent for $\eta=-1$. This happens because anticorrelated broadening effects between the peaks reverses the rephasing of oscillators. As a result, pathways in which frequency fluctuations during t_1 and t_3 are anticorrelated do not show a photon echo. The corresponding mixed time-frequency plots [Eq. (45)], are shown in Figs. 4(b), 5(b), and 6(b). These trends are seen in all three techniques: The slow bath plots [first row Fig. 4(a)] show beats in the correlated signal for $\mathbf{k_I}$. These beats are reduced in the anticorrelated case, indicating the absence of an echo. We still see a signal corresponding to the diagonal peaks since there is an echo for vibronic pathways involving correlated signals in the first and third time intervals. The reverse is true for techniques $\mathbf{k_{II}}$ and $\mathbf{k_{III}}$ where no echo is expected. The anticorrelation between energy levels reverses the dephasing of oscillators and an echo is formed for vibronic pathways involving anticorrelated frequency fluctuations in the first and third time intervals. This results in well-resolved anticorrelated cross peaks [first row: Figs. 5(a) and 6(b)]. The mixed time frequency plots [first row: Figs. 5(b) and 6(b)] show this effect more clearly. The signal dephases rapidly for the correlated and uncorrelated cases along the t_1 axis but remains strong for the anticorrelated case. As κ is increased, the line shape crosses over from a Gaussian to a Lorentzian profile and all correlation effects gradually disappear.

The $\mathbf{k_I}$, $\mathbf{k_{II}}$, and $\mathbf{k_{III}}$ signals are displayed on a linear scale in Figs. 7, 8, and 9. The plots have been normalized by setting the strongest peak strength in each frame to 1. The strong features are best resolved on the linear scale. The log scale plots which have not been normalized enable the comparison of the relative peaks strengths for different techniques and show the weak features in more detail. The resolution of the peaks can be improved by looking at the real part of the signal which adds up the purely absorptive amplitudes giving well localized peaks (the imaginary part, on the other hand, emphasizes the dispersive terms, resulting in a more diffuse spectrum). Complete sets of normalized plots for (a) the real [Eq. (47)] and (b) the imaginary part [Eq. (48)] of the signals $\mathbf{k_I}$, $\mathbf{k_{II}}$, and $\mathbf{k_{III}}$ are presented in Figs. 10, 11, and 12 as supplementary material.[42]

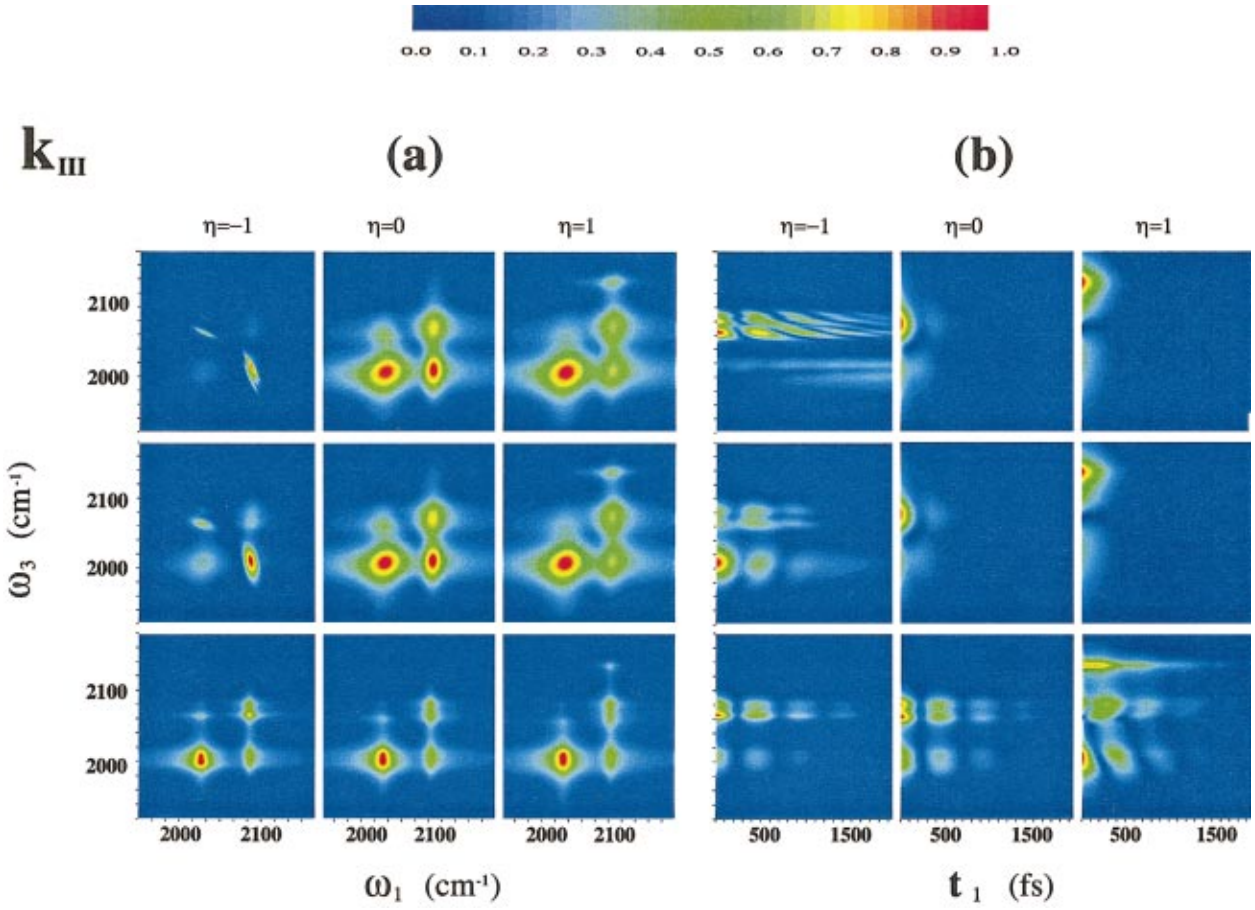

FIG. 9. (Color) Same as Fig. 7 but for $\mathbf{k_{III}}$.

S_s^R [Figs. 10(a), 11(a), and 12(a)] shows well resolved peaks for all techniques as all nonlocal dispersive features have been filtered out. The negative peaks correspond to Liouville space pathways involving single to double exciton transitions during t_3. $\mathbf{k_{II}}$ and $\mathbf{k_{III}}$ show some background reflecting the large nonrephasing diagonal terms. For S_s^I [Figs. 10(b), 11(b), and 12(b)], the sum of closely separated dispersive components with opposite signs, leads to large negative peaks surrounded by two positive peaks on either side. The background is very diffuse stemming from the interference of long dispersive tails.

In summary we have identified several specific signatures of bath couplings in third order 2D spectroscopies. The energy level fluctuation parameters used in our calculations may be directly obtained from molecular dynamics simulations. The present model assumes fluctuations around a single stable structure. For molecules such as peptides[43] with several interconverting structures, it may become necessary to switch to a time dependent reference structure and calculate the spectra using an adiabatic representation.[44,45]

The theory developed in Ref. 28 also allows for vibrational relaxation during the interval t_2 introduced by the off-diagonal components of the system bath coupling term H_{0e} in the exciton basis set. Vibrational relaxation does not affect the 2D signals calculated here for $t_2=0$. A study of the time evolution of the signal during t_2 in a three pulse experiment showed population relaxation effects which induce a redistribution of intensities among the cross peaks.[41] Including the off-diagonal elements to study the effect of the bath on vibrational relaxation should be an interesting future extension of the present work.

ACKNOWLEDGMENTS

The support of the National Institutes of Health (GM59230-01A2) and the National Science Foundation (CHE-0132571) is gratefully acknowledged.

APPENDIX A: TRANSFORMING THE LINE BROADENING FUNCTIONS TO THE EXCITON BASIS

Equations (20) and (21) transform the Hamiltonian from the localized to the exciton basis set. The bath coordinates transform as follows

$$q_{\alpha\beta}^{(c)}=\sum_{mn=1}^{N}\phi_{\alpha,m}\phi_{\beta,n}q_{mn}^{(c)}, \tag{A1}$$

$$q_{\mu\nu}^{(c)}=\sum_{\substack{mnkl=1\\ n\geqslant m\\ l\geqslant k}}^{N} q_{mnkl}^{(c)}\psi_{\mu,mn}\psi_{\nu,kl}. \tag{A2}$$

The system-bath coupling is given by

$$H_{ce}=\sum_{\alpha\beta} q_{\alpha\beta}^{(c)}B_\alpha^\dagger B_\beta+\sum_{\mu\nu} q_{\mu\nu}^{(c)}Y_\mu^\dagger Y_\nu, \tag{A3}$$

where $q_{\alpha\beta}^{(c)}$ and $q_{\mu\nu}^{(c)}$ are transformed collective coordinates.

APPENDIX B: THE FOUR POINT CORRELATION FUNCTION

In Sec. III we defined two four point correlation functions: F_1 only depends on single exciton states and F_2 also depends on double exciton states. Using the procedure outlined in Sec. III leads to the following expressions:

$$F_1(\tau_4,\tau_3,\tau_2,\tau_1)=\sum_{\alpha\beta} d_\alpha d_\alpha d_\beta d_\beta \exp(-iE_\beta(\tau_4-\tau_3)-iE_\alpha(\tau_2-\tau_1))\exp(-g_{\beta\beta}(\tau_4-\tau_3)+g_{\beta\alpha}(\tau_4-\tau_2)$$
$$-g_{\beta\alpha}(\tau_3-\tau_2)+g_{\beta\alpha}(\tau_3-\tau_1)-g_{\alpha\alpha}(\tau_2-\tau_1)+g_{\beta\alpha}(\tau_4-\tau_1)) \tag{B1}$$

and

$$\begin{aligned}F_2(\tau_4,\tau_3,\tau_2,\tau_1)=&\sum_{\substack{\alpha\beta\gamma\mu\delta\\ \gamma\geqslant\delta}} d_\alpha d_\beta d_\gamma d_\delta \exp(-iE_\delta(\tau_4-\tau_3)-iE_\mu(\tau_3-\tau_2)-iE_\beta(\tau_2-\tau_1))\exp(g_{\delta\mu}(\tau_4-\tau_3)-g_{\delta\delta}(\tau_4-\tau_3)\\
&-g_{\delta\mu}(\tau_4-\tau_2)+g_{\delta\beta}(\tau_4-\tau_2)-g_{\mu\mu}(\tau_3-\tau_2)+g_{\mu\beta}(\tau_3-\tau_2)\\
&+g_{\delta\mu}(\tau_3-\tau_2)-g_{\delta\beta}(\tau_3-\tau_2)-g_{\delta\beta}(\tau_4-\tau_1)-g_{\mu\beta}(\tau_3-\tau_1)+g_{\delta\beta}(\tau_3-\tau_1)\\
&+g_{\mu\beta}(\tau_2-\tau_1)-g_{\beta\beta}(\tau_2-\tau_1))\chi_{\mu,\alpha\beta}\chi'_{\mu,\delta\gamma}+\sum_{\substack{\alpha\beta\gamma\mu\delta\\ \delta\geqslant\gamma}} d_\alpha d_\beta d_\gamma d_\delta \exp(-iE_\delta(\tau_4-\tau_3)-iE_\mu(\tau_3-\tau_2)\\
&-iE_\beta(\tau_2-\tau_1))\exp(g_{\delta\mu}(\tau_4-\tau_3)-g_{\delta\delta}(\tau_4-\tau_3)-g_{\delta\mu}(\tau_4-\tau_2)+g_{\delta\beta}(\tau_4-\tau_2)-g_{\mu\mu}(\tau_3-\tau_2)\\
&+g_{\mu\beta}(\tau_3-\tau_2)+g_{\delta\mu}(\tau_3-\tau_2)-g_{\delta\beta}(\tau_3-\tau_2)-g_{\delta\beta}(\tau_4-\tau_1)-g_{\mu\beta}(\tau_3-\tau_1)+g_{\delta\beta}(\tau_3-\tau_1)\\
&+g_{\mu\beta}(\tau_2-\tau_1)-g_{\beta\beta}(\tau_2-\tau_1))\chi_{\mu,\alpha\beta}\chi'_{\mu,\gamma\delta},\end{aligned} \tag{B2}$$

where $\chi_{\mu,\alpha\beta}$ and $\chi'_{\mu,\alpha\beta}$ are expansion coefficients defined in Eqs. (36) and (37). The line broadening functions g are defined as

$$g_{ab}(\tau)=\int_0^\tau d\tau_1\int_0^{\tau_1} d\tau_2 C_{ab}(\tau_2). \tag{B3}$$

Using the definition of the C's [Eq. (38)] we get

$$g_{ab}(\tau)=\frac{2K_BT\lambda_{ab}}{\hbar\Lambda_{ab}^2}(\exp(-\Lambda_{ab}\tau)+\Lambda_{ab}\tau-1)-i\left(\frac{\lambda_{ab}}{\Lambda_{ab}}\right)(\exp(-\Lambda_{ab}\tau)+\Lambda_{ab}\tau-1). \tag{B4}$$

The transformation equations to obtain the line broadening functions in the exciton basis are as given in the following. We use the following shorthand notation: $g_{ab}\equiv g_{aabb}$, where a and b could represent either single or double exciton states:

$$g_{\alpha\beta}=g_{\beta\alpha}=\sum_{mnkl=1}^{N} g_{mnkl}(t)\phi_{\alpha,m}\phi_{\alpha,n}\phi_{\beta,k}\phi_{\beta,l}, \tag{B5}$$

$$g_{\mu\alpha}=g_{\alpha\mu}=\sum_{\substack{mn=1\\ n'\geqslant m'\\ l'\geqslant k'}}^{N}\sum_{m'n'k'l'=1} g_{mnm'n'k'l'}(t)\times\phi_{\alpha,m}\phi_{\alpha,n}\psi_{\mu,m'n'}\psi_{\mu,k'l'}, \tag{B6}$$

$$g_{\mu\nu}=g_{\nu\mu}=\sum_{\substack{mnlk=1\\ n\geqslant m\ \ l\geqslant k\\ n'\geqslant m'\ \ l'\geqslant k'}}^{N}\sum_{m'n'k'l'=1} g_{mnklm'n'k'l'}(t)\times\psi_{\mu,mn}\psi_{\mu,kl}\psi_{\nu,m'n'}\psi_{\nu,k'l'}. \tag{B7}$$

APPENDIX C: LIMITING CASES FOR THE FOUR POINT CORRELATION FUNCTIONS

In the slow bath limit ($\kappa\ll 1$) the line broadening function becomes $g_{ab}(t)=\Delta_{ab}^2t^2/2$. Equations (B1) and (B2) reduce to the form

$$F_1(\tau_4,\tau_3,\tau_2,\tau_1)=\sum_{\alpha\beta} d_\alpha d_\alpha d_\beta d_\beta \exp(-iE_\beta(\tau_4-\tau_3)-iE_\alpha(\tau_2-\tau_1))$$
$$\times\exp(-\Delta^2_{\beta\beta}(\tau_4-\tau_3)^2+\Delta^2_{\alpha\alpha}(\tau_2-\tau 1)^2-\Delta^2_{\beta\alpha}((\tau_4-\tau_3)(\tau_2-\tau_1)) \tag{C1}$$

and

$$F_2(\tau_4,\tau_3,\tau_2,\tau_1)=\sum_{\substack{\alpha\beta\gamma\mu\delta\\ \gamma\geqslant\delta}} d_\alpha d_\beta d_\gamma d_\delta \exp(-iE_\delta(\tau_4-\tau_3)-iE_\mu(\tau_3-\tau_2)$$
$$-iE_\beta(\tau_2-\tau_1))\exp(\Delta^2_{\delta\delta}(\tau_4-\tau_3)^2-\Delta^2_{\mu\mu}(\tau_3-\tau_2)^2-\Delta^2_{\beta\beta}(\tau_2-\tau_1)^2-2\Delta^2_{\delta\mu}(\tau_4-\tau_3)(\tau_3-\tau_2)$$
$$-2\Delta^2_{\delta\beta}(\tau_2-\tau_1)(\tau_4-\tau_3))\chi_{\mu,\alpha\beta}\chi'_{\mu,\delta\gamma}+\sum_{\substack{\alpha\beta\gamma\mu\delta\\ \delta\geqslant\gamma}} d_\alpha d_\beta d_\gamma d_\delta \exp(-iE_\delta(\tau_4-\tau_3)-iE_\mu(\tau_3-\tau_2)$$
$$-iE_\beta(\tau_2-\tau_1))\exp(\Delta^2_{\delta\delta}(\tau_4-\tau_3)^2-\Delta^2_{\mu\mu}(\tau_3-\tau_2)^2-\Delta^2_{\beta\beta}(\tau_2-\tau_1)^2-2\Delta^2_{\delta\mu}(\tau_4-\tau_3)(\tau_3-\tau_2)$$
$$-2\Delta^2_{\delta\beta}(\tau_2-\tau_1)(\tau_4-\tau_3))\chi_{\mu,\alpha\beta}\chi'_{\mu,\gamma\delta}. \tag{C2}$$

In the fast bath limit ($\kappa\gg 1$) the line broadening function becomes $g_{ab}(t)=(\Gamma_{ab}-i\lambda_{ab})t$ where $\Gamma_{ab}=\Delta^2_{ab}/2$. Equations (B1) and (B2) then assume the form

$$F_1(\tau_4,\tau_3,\tau_2,\tau_1)=\sum_{\alpha\beta} d_\alpha d_\alpha d_\beta d_\beta \exp(-iE_\beta(\tau_4-\tau_3)-iE_\alpha(\tau_2-\tau_1))$$
$$\times\exp(-(\Gamma_{\beta\beta}-i\lambda_{\beta\beta})(\tau_4-\tau_3)-(\Gamma_{\alpha\alpha}-i\lambda_{\alpha\alpha})(\tau_2-\tau_1)) \tag{C3}$$

and

$$F_2(\tau_4,\tau_3,\tau_2,\tau_1)=\sum_{\substack{\alpha\beta\gamma\mu\delta\\ \gamma\geqslant\delta}} d_\alpha d_\beta d_\gamma d_\delta \exp(-iE_\delta(\tau_4-\tau_3)-iE_\mu(\tau_3-\tau_2)$$
$$-iE_\beta(\tau_2-\tau_1))\exp(-(\Gamma_{\delta\delta}-i\lambda_{\delta\delta})(\tau_4-\tau_3)-(\Gamma_{\mu\mu}-i\lambda_{\mu\mu})(\tau_3-\tau_2)-(\Gamma_{\beta\beta}-i\lambda_{\beta\beta})(\tau_2-\tau_1))$$
$$\times\chi_{\mu,\alpha\beta}\chi'_{\mu,\delta\gamma}$$
$$+\sum_{\substack{\alpha\beta\gamma\mu\delta\\ \delta\geqslant\gamma}} d_\alpha d_\beta d_\gamma d_\delta \exp(-iE_\delta(\tau_4-\tau_3)-iE_\mu(\tau_3-\tau_2)-iE_\beta(\tau_2-\tau_1))\times\exp(-(\Gamma_{\delta\delta}-i\lambda_{\delta\delta})(\tau_4-\tau_3)$$
$$-(\Gamma_{\mu\mu}-i\lambda_{\mu\mu})(\tau_3-\tau_2)-(\Gamma_{\beta\beta}-i\lambda_{\beta\beta})(\tau_2-\tau_1))\chi_{\mu,\alpha\beta}\chi'_{\mu,\gamma\delta}. \tag{C4}$$

APPENDIX D: BROADENING PARAMETERS FOR THE TWO COUPLED VIBRATIONS MODEL

We can express all fluctuation amplitudes and their correlations in terms of the two independent fluctuations and η defined in Sec. V.

$$\Delta^2_{12}=\eta\Delta_{11}\Delta_{22},\quad \Delta^2_{(12)',(12)'}=\Delta^2_{11}+\Delta^2_{22}+2\eta\Delta_{11}\Delta_{22},$$
$$\Delta^2_{1'2'}=4\eta\Delta_{11}\Delta_{22},\quad \Delta^2_{1'(12)'}=2(\Delta^2_{11}+\eta\Delta_{11}\Delta_{22}),$$
$$\Delta^2_{2'(12)'}=2(\Delta^2_{22}+\eta\Delta_{11}\Delta_{22}),\quad \Delta^2_{11'}=2\Delta^2_{11}, \tag{D1}$$
$$\Delta^2_{12'}=2\eta\Delta_{11}\Delta_{22},\quad \Delta^2_{1(12)'}=\Delta^2_{11}+\eta\Delta_{11}\Delta_{22},$$
$$\Delta^2_{2(12)'}=\Delta^2_{22}+\eta\Delta_{11}\Delta_{22},\quad \Delta^2_{21'}=2\eta\Delta_{11}\Delta_{22},$$
$$\Delta^2_{22'}=2\Delta^2_{22}$$

with $\Delta^2_{ab}=\Delta^2_{ba}$.

[1] R. R. Ernst, G. Bodenhausen, and A. Wokaun, *Principles of Nuclear Magnetic Resonance in One and Two Dimensions* (Clarendon, Oxford, 1987).
[2] L. Emsley and A. Pines, *Lectures on Pulsed NMR*, 2nd ed., ''Nuclear Magnetic Double Resonance, Proceedings of the CXXIII School of Physics ''Enrico Fermi'' (World Scientific, Amsterdam, 1993).
[3] Y. Tanimura and S. Mukamel, J. Chem. Phys. **99**, 9496 (1993).
[4] S. Mukamel, Annu. Rev. Phys. Chem. **51**, 691 (2000).
[5] M. T. Zanni, N. Ge, Y. S. Kim, and R. M. Hochstrasser, Proc. Natl. Acad. Sci. U.S.A. **98**, 11265 (2001).
[6] D. Zimdars, A. Tokmakoff, S. Chen, S. R. Greenfield, M. D. Fayer, T. I. Smith, and H. A. Schwettman, Phys. Rev. Lett. **70**, 2718 (1993).
[7] P. Hamm, M. Lim, W. F. Degrado, and R. M. Hochstrasser, J. Chem. Phys. **112**, 1907 (2000).
[8] M. C. Asplund, M. T. Zanni, and R. M. Hochstrasser, Proc. Natl. Acad. Sci. U.S.A. **97**, 8219 (2000).
[9] K. D. Rector, D. E. Thompson, K. Merchant, and M. D. Fayer, Chem. Phys. Lett. **316**, 122 (2000).
[10] N. Ge, M. T. Zanni, and R. M. Hochstrasser, J. Phys. Chem. A **106**, 962 (2002).
[11] N. Ge and R. M. Hochstrasser, Phys. Chem. Commun. **3**, 1 (2002).
[12] S. Woutersen, Y. Mu, G. Stock, and P. Hamm, Proc. Natl. Acad. Sci. U.S.A. **98**, 11254 (2002).

[13] S. Mukamel, A. Piryatinski, and V. Chernyak, Acc. Chem. Res. **32**, 145 (1999).
[14] D. A. Blank, L. J. Kaufman, and G. R. Fleming, J. Chem. Phys. **111**, 3105 (1999).
[15] K. J. Kubarych, C. J. Milne, S. Lin, V. Astinov, and R. J. D. Miller, J. Chem. Phys. **116**, 2016 (2002).
[16] T. I. C. Jansen, J. G. Snijders, and K. Duppen, J. Chem. Phys. **114**, 10910 (2001).
[17] K. Okumura, A. Tokmakoff, and Y. Tanimura, J. Chem. Phys. **111**, 492 (1999).
[18] L. J. Kaufman, J. Heo, G. R. Fleming, J. Sung, and M. Cho, Chem. Phys. **266**, 251 (2001).
[19] J. E. Ivanecky and J. C. Wright, Chem. Phys. Lett. **206**, 437 (1993).
[20] S. Mukamel and R. Hochstrasser, editors, Special issue Chem. Phys. **266**, 135 (2001).
[21] P. Hamm, M. Lim, and R. M. Hochstrasser, Phys. Rev. Lett. **81**, 5326 (1998).
[22] D. Oron, N. Dudovich, D. Yelin, and Y. Silberberg, Phys. Rev. A **65**, 043408 (2002).
[23] C. Scheurer and S. Mukamel, J. Chem. Phys. **115**, 4989 (2001).
[24] D. Zeidler, S. Frey, W. Wohlleben, M. Motzkus, F. Busch, T. Chen, W. Keifer, and A. Materny, J. Chem. Phys. **116**, 5231 (2002).
[25] T. Brixner and G. Gerber, Opt. Lett. **26**, 557 (2001); A. Assion, T. Baumert, M. Bergt, T. Brixner, B. Keifer, V. Seyfried, M. Strehle, and G. Gerber, Science **282**, 919 (1998).
[26] R. J. Levis and H. Rabitz, J. Phys. Chem. (to be published).
[27] S. Mukamel, Phys. Rev. A **28**, 3480 (1983).
[28] T. Meier, V. Chernyak, and S. Mukamel, J. Chem. Phys. **107**, 8759 (1997).
[29] W. M. Zhang, T. Meier, V. Chernyak, and S. Mukamel, J. Chem. Phys. **108**, 7763 (1998).
[30] R. Venkatramani and S. Mukamel, Ultrafast Phenomena XII, edited by R. J. Miller, M. M. Murnane, N. F. Scherer, and A. M. Wiener (Springer-Verlag, Berlin, 2002).
[31] S. Mukamel, *Principles of Nonlinear Optical Spectroscopy* (Oxford University Press, New York, 1995).
[32] A. Wünsche, J. Opt. B: Quantum Semiclassical Opt. **1**, 264 (1999).
[33] N. Demirdöven, M. Khalil, O. Golonzka, and A. Tokmakoff, J. Phys. Chem. A **105**, 8025 (2001).
[34] D. E. Thompson, K. A. Merchant, and M. D. Fayer, J. Chem. Phys. **115**, 317 (2001).
[35] S. Mukamel, A. Piryatinski, and V. Chernyak, J. Chem. Phys. **110**, 1711 (1999); K. Okumura and Y. Tanimura, Chem. Phys. Lett. **278**, 175 (1997).
[36] T. Steffen and Y. Tanimura, J. Phys. Soc. Jpn. **69**, 3115 (2000).
[37] Y. Tanimura and T. Steffen, J. Phys. Soc. Jpn. **69**, 4095 (2000).
[38] S. Gnanakaran and R. M. Hochstrasser, J. Am. Chem. Soc. **123**, 12886 (2001).
[39] A. Piryatinski, S. Tretiak, V. Chernyak, and S. Mukamel, J. Raman Spectrosc. **31**, 125 (2000).
[40] S. Mukamel, Phys. Rep. **93**, 1 (1982).
[41] A. Piryatinski, V. Chernyak, and S. Mukamel, Chem. Phys. **266**, 285 (2000).
[42] See EPAPS Document No. E-JCPSA6-117-002246 for normalized plots of the real and imaginary part of the signals $\mathbf{k_I}$, $\mathbf{k_{II}}$, and $\mathbf{k_{III}}$. A direct link to this document may be found in the online article's HTML reference section. The document may also be reached via the EPAPS homepage (http://www.aip.org/pubservs/epaps.html) or from ftp.aip.org in the directory /epaps/. See the EPAPS homepage for more information.
[43] S. Spörlein, H. Carstens, C. Renner, R. Behrendt, L. Moroder, P. Tavan, W. Zinth, and J. Wachtveitl, Proc. Natl. Acad. Sci. U.S.A. (to be published).
[44] J. W. Zwanziger, M. Koenig, and A. Pines, Annu. Rev. Phys. Chem. **41**, 601 (1990).
[45] F. Wilczek and A. Zee, Phys. Rev. Lett. **52**, 2111 (1984).